SUPPORTING INFORMATION

Intramolecular Charge Transfer and Ultrafast Nonradiative Decay in DNA-Tethered Asymmetric Nitro- and Dimethylamino-Substituted Squaraines

Nicholas D. Wright,[1] Jonathan S. Huff,[1] Matthew S. Barclay,[1] Christopher K. Wilson,[1] German Barcenas,[1] Katelyn M. Duncan,[1] Maia Ketteridge,[1] Olena M. Obukhova,[2] Alexander I. Krivoshey,[2] Anatoliy L. Tatarets,[2] Ewald A. Terpetschnig,[3] Jacob C. Dean,[4] William B. Knowlton,[1,5] Bernard Yurke, [1,5] Lan Li,[1,6] Olga A. Mass,[1] Paul H. Davis,[1,6] Jeunghoon Lee,[1,7] Daniel B. Turner,[1] Ryan D. Pensack[1]

[1]Micron School of Materials Science & Engineering, [5]Department of Electrical & Computer Engineering, [7]Department of Chemistry & Biochemistry, Boise State University, Boise, Idaho 83725, United States

[2]SSI "Institute for Single Crystals" of the National Academy of Sciences of Ukraine, Kharkiv 61072, Ukraine

[3]SETA BioMedicals, Urbana, Illinois 61801, United States

[4]Department of Physical Science, Southern Utah University, Cedar City, Utah 84720, United States

[6]Center for Advanced Energy Studies, Idaho Falls, Idaho 83401, United States

Table of Contents:

Section S10. Supporting References

1. Squaraine Synthesis and Characterization

General

The **C, H, N elemental analysis** was performed using an EuroVector Euro EA 3000 EA-IRMS elemental analyzer.

^{1}H NMR spectra were measured on a Varian 400 MR (^{1}H 400 MHz) spectrometer in DMSO-d_6 using the signal of the remaining non-deuterated solvent as an internal standard (2.50 ppm for DMSO).[S1]

ESI mass spectra were recorded on a *Waters Quattro micro API* mass spectrometer with direct injection of the sample solution to the ionization chamber. Spectra were recorded in ESI$^+$ at 120 °C with energy 3 kV on capillary.

Absorption spectra were recorded in 1-cm quartz cells at 25 ºC using a PerkinElmer Lambda 35 UV/Vis spectrophotometer. Absorption maxima were determined with an accuracy of ±0.5 nm and rounded off.

Specific

2-((1-(5-carboxypentyl)-3,3-dimethylindolin-2-ylidene)methyl)-3-oxo-4-((1,3,3-trimethyl-5-dimethylamino-3*H*-indol-1-ium-2-yl)methylene)cyclobut-1-en-1-olate (2-COOH)

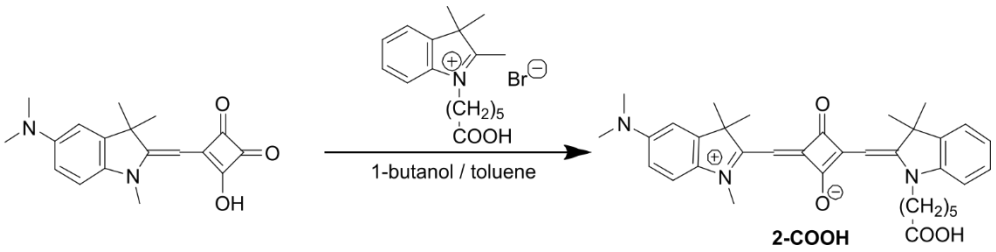

3-((5-(Dimethylamino)-1,3,3-trimethylindolin-2-ylidene)methyl)-4-hydroxycyclobut-3-ene-1,2-dione (200 mg, 0.64 mmol) and 1-(5-carboxypentyl)-2,3,3-trimethyl-3H-indolium bromide (230 mg, 0.65 mmol) were heated under reflux in toluene (8 mL) and 1-butanol (10 mL) for 2 h. The solvents were removed under reduced pressure by a rotary evaporator. Acetic acid (15 mL) and concentrated hydrochloric acid (1.5 mL) were added to the residue and refluxed for 1 hour. The acids were rotary evaporated and the obtained raw product was purified by column chromatography (Silica gel 60, 0–5 % methanol—chloroform) to give **2-COOH** (95 mg, 26 %). ^{1}H-NMR (400 MHz, DMSO-d$_6$), δ, ppm: 7.43 (1H, d, 7.2 Hz, arom.), 7.28 (1H, dd, J_1 = 8.0 Hz, J_2 < 1.0 Hz, arom.), 7.25 (1H, d, 8.9 Hz, arom.), 7.17 (1H, d, 7.8 Hz, arom.), 7.06 (1H, dd, J_1 = 7.5 Hz, J_2 < 1.0 Hz, arom.), 6.97 (1H, d, 2.4 Hz, arom.), 6.70 (1H, dd, J_1 = 8.8 Hz, J_2 =2.4 Hz, arom.), 5.74 (1H, s, CH), 5.65 (1H, s, CH), 3.95 (2H, broad s, NCH_2), 3.60 (3H, s, NCH_3), 2.95 (6H, s, $N(CH_3)_2$), 2.21 (2H, t, 7.1 Hz, $C\underline{H}_2COOH$), 1.68 (6H, s, $(CH_3)_2$), 1.65 (6H, s, $(CH_3)_2$), 1.60–1.32 (6H, m, CH_2). ESI MS, m/z calcd. for $[M+H]^+$ $[C_{35}H_{42}N_3O_4]^+$ 568.32, found: 568.34. Anal. calcd.

(%) for $C_{35}H_{41}N_3O_4$: C, 74.05; H, 7.28; N, 7.40. Found C, 73.93; H, 7.23; N, 7.49. UV-Vis: λ_{max}(Abs) 645 nm, ε 124,000 $M^{-1}cm^{-1}$ (Methanol).

4-((5-(dimethylamino)-1,3,3-trimethyl-3*H*-indol-1-ium-2-yl)methylene)-2-((1-(6-((2,5-dioxopyrrolidin-1-yl)oxy)-6-oxohexyl)-3,3-dimethylindolin-2-ylidene)methyl)-3-oxocyclobut-1-en-1-olate (2-NHS)

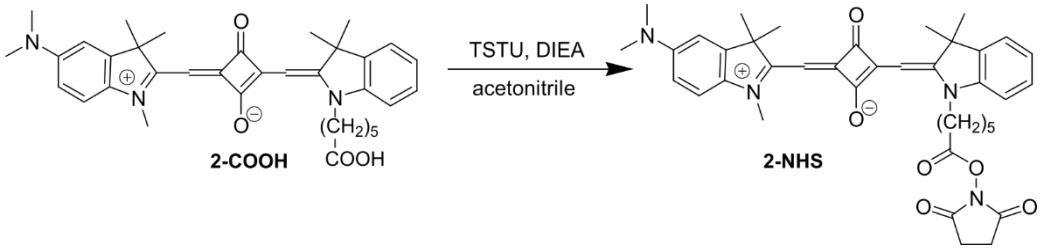

2-COOH (27 mg, 47 μmol), and *N*,*N*,*N*′,*N*′-tetramethyl-*O*-(*N*-succinimidyl)uronium tetrafluoroborate (TSTU) (42 mg, 140 μmol) were dissolved in acetonitrile (2.5 mL) and chloroform (0.5 mL), and *N*,*N*-diisopropylethylamine (DIEA) (24 μL, 140 μmol) were added. The solution was stirred at room temperature for 30 min, the solvents were removed under reduced pressure by rotary evaporation and the residue was purified by column chromatography (Silica gel 60, 0.5–1% methanol—chloroform) to yield 21 mg (66 %) **2-NHS**. ^{1}H-NMR (400 MHz, DMSO-d_6), δ, ppm: 7.43 (1H, d, 7.0 Hz, arom.), 7.29 (1H, dd, J_1 = 7.9 Hz, J_2 < 1.0 Hz, arom.), 7.24 (1H, d, 8.6 Hz, arom.), 7.17 (1H, d, 7.6 Hz, arom.), 7.07 (1H, dd, J_1 = 7.1 Hz, J_2 < 1.0 Hz, arom.), 6.98 (1H, s, arom.), 6.71 (1H, d, 8.7 Hz, arom.), 5.74 (1H, s, CH), 5.65 (1H, s, CH), 3.95 (2H, broad s, NCH_2), 3.60 (3H, s, NCH_3), 2.95 (6H, s, $N(CH_3)_2$), 2.82 (4H, s, CH_2 (succinimide)), 2.69 (2H, t, 7.7 Hz, CH_2COONHS), 1.76–1.45 (6H, m, CH_2), 1.68 (6H, s, $(CH_3)_2$), 1.65 (6H, s, $(CH_3)_2$). ESI MS, m/z calcd. for $[M+H]^+$ $[C_{39}H_{45}N_4O_6]^+$ 665.33, found: 665.44. Anal. calcd. (%) for $C_{39}H_{44}N_4O_6$: C, 70.46; H, 6.67; N, 8.43. Found C, 70.41; H, 6.63; N, 8.38. UV-Vis: λ_{max}(Abs) 645 nm, ε 124,000 $M^{-1}cm^{-1}$ (Methanol).

2-((1-(5-carboxypentyl)-3,3-dimethylindolin-2-ylidene)methyl)-3-oxo-4-((1,3,3-trimethyl-5-nitro-3*H*-indol-1-ium-2-yl)methylene)cyclobut-1-en-1-olate (3-COOH)

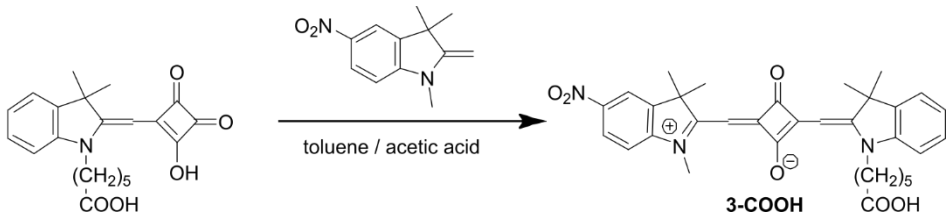

3-Hydroxy-4-(1-(5-carboxypentyl)-(1,3,3-trimethylindolin-2-ylidene)methyl)cyclobut-3-ene-1,2-dione (**1**) (116 mg, 0.31 mmol) and 1,3,3-trimethyl-2-methylene-5-nitroindoline (**2**) (68 mg, 0.31 mmol) were heated under reflux in a mixture of toluene (20 mL) and acetic acid (5 mL) for 8 h. The solvents was removed under reduced pressure with a rotary evaporator and the residue was purified by column chromatography (Silica gel 60, 5–10 % methanol—chloroform) to give **3-COOH** (74 mg, 42%). ^{1}H-NMR (400 MHz, DMSO-d_6), δ, ppm: 8.31 (1H, s, arom.), 8.24 (1H, d,

8.5 Hz, arom.), 7.61 (1H, d, 6.8 Hz, arom.), 7.50 (1H, d, 7.9 Hz, arom.), 7.42 (1H, t, 7.6 Hz, arom.), 7.37 (1H, d, 8.7 Hz, arom.), 7.29 (1H, t, 7.6 Hz, arom.), 5.99 (1H, s, CH), 5.80 (1H, s, CH), 4.22 (1H, t, 6.2 Hz, NCH_2), 3.52 (3H, s, NCH_3), 2.21 (2H, t, 6.9 Hz, $C\underline{H_2}COOH$), 1.72 (12H, s, $(CH_3)_2$), 1.81–1.65 (2H, m CH_2), 1.61–1.50 (2H, m CH_2), 1.46–1.34 (2H, m CH_2). ESI MS, m/z calcd. for $[M+H]^+$ $[C_{33}H_{36}N_2O_4]^+$ 570.26, found: 570.32. Anal. calcd. (%) for $C_{33}H_{35}N_3O_6$: C, 69.58; H, 6.19; N, 7.38. Found C, 69.43; H, 6.18; N, 7.40. UV-Vis: λ_{max}(Abs) 637 nm, ε 170,000 $M^{-1}cm^{-1}$ (Methanol).

2-((1-(6-((2,5-dioxopyrrolidin-1-yl)oxy)-6-oxohexyl)-3,3-dimethylindolin-2-ylidene)methyl)-3-oxo-4-((1,3,3-trimethyl-5-nitro-3H-indol-1-ium-2-yl)methylene)cyclobut-1-en-1-olate (3-NHS)

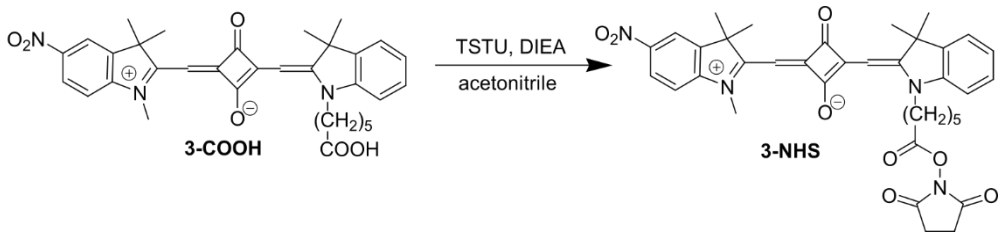

3-COOH (30 mg, 58 μmol), *N*,*N*,*N*′,*N*′-tetramethyl-*O*-(*N*-succinimidyl)uronium tetrafluoroborate (TSTU) (23 mg, 76 μmol) were dissolved in acetonitrile (3 mL) and chloroform (0.5 mL), and then *N*,*N*-diisopropylethylamine (DIEA) (17 μL, 97 μmol) was added. The solution was stirred at room temperature for 20 min. The solvent was removed under reduced pressure by a rotary evaporator and the residue was purified using column chromatography (Silica gel 60, 0.5–1% methanol—chloroform) to yield 22 mg (57 %) **3-NHS**. ^{1}H-NMR (400 MHz, DMSO-d_6), δ, ppm: 8.35 (1H, s, arom.), 8.24 (1H, d, 9.1 Hz, arom.), 7.61 (1H, d, 7.8 Hz, arom.), 7.50 (1H, d, 7.5 Hz, arom.), 7.42 (1H, t, 7.4 Hz, arom.), 7.37 (1H, d, 9.0 Hz, arom.), 7.29 (1H, t, 7.8 Hz, arom.), 5.99 (1H, s, CH), 5.80 (1H, s, CH), 4.22 (1H, t, 6.9 Hz, NCH_2), 3.52 (3H, s, NCH_3), 2.83 (4H, s, CH_2 (succinimide)), 2.69 (2H, t, 7.8 Hz, $C\underline{H_2}COONHS$), 1.84–1.75 (2H, m, CH_2), 1.72 (12H, s, $(CH_3)_2$), 1.59–1.46 (2H, m CH_2), 1.42–1.30 (2H, m CH_2). ESI MS, m/z calcd. for $[M+H]^+$ $[C_{37}H_{39}N_4O_8]^+$ 667.28, found: 667.37. Anal. calcd. (%) for $C_{37}H_{38}N_4O_8$: C, 66.65; H, 5.75; N, 8.40. Found C, 66.34; H, 5.70; N, 8.29. UV-Vis: λ_{max}(Abs) 637 nm, ε 170,000 $M^{-1}cm^{-1}$ (Methanol).

2-((1-(5-carboxypentyl)-3,3-dimethyl-5-nitroindolin-2-ylidene)methyl)-4-((5-(dimethylamino)-1,3,3-trimethyl-3*H*-indol-1-ium-2-yl)methylene)-3-oxocyclobut-1-en-1-olate (4-COOH)

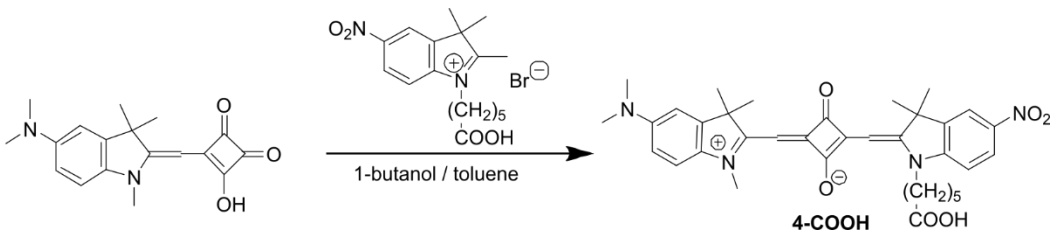

3-((5-(Dimethylamino)-1,3,3-trimethylindolin-2-ylidene)methyl)-4-hydroxycyclobut-3-ene-1,2-dione (50 mg, 0.16 mmol) and 1-(5-carboxypentyl)-2,3,3-trimethyl-5-nitro-3*H*-indolium bromide 130 mg (0.325 mmol) were heated under reflux in a mixture of toluene (4 mL) and 1-butanol (5 mL) for 2.5 h. The solvents were removed under reduced pressure by rotary evaporation. Acetic acid (10 mL) and concentrated hydrochloric acid (1.0 mL) were added to the residue and the mixture was refluxed for 40 min, and the reaction was monitored by TLC. The acids were removed by a rotary evaporator and the obtained raw product was purified by a column chromatography (Lihroprep RP-18, 45–50 % acetonitrile—water) to give **4-COOH** (10.5 mg, 11 %). ^{1}H-NMR (400 MHz, DMSO-d_6), δ, ppm: 8.24 (1H, s, arom.), 8.19 (1H, d, 8.1 Hz, arom.), 7.40 (1H, d, 8.8 Hz, arom.), 7.24 (1H, d, 8.0 Hz, arom.), 7.01 (1H, s, arom.), 6.75 (1H, d, 7.8 Hz, arom.), 5.93 (1H, s, CH), 5.72 (1H, s, CH), 3.94 (1H, t, 6.4 Hz, NCH_2), 3.74 (3H, s, NCH_3), 2.98 (6H, s, $N(CH_3)_2$), 2.21 (2H, t, 7.1 Hz, $C\underline{H}_2COOH$), 1.71 (6H, s, $(CH_3)_2$), 1.69 (6H, s, $(CH_3)_2$), 1.60–1.30 (6H, m CH_2). ESI MS, m/z calcd. for $[M+H]^+$ $[C_{35}H_{41}N_4O_6]^+$ 613.30, found: 613.38. Anal. calcd. (%) for $C_{35}H_{40}N_4O_6$: C, 68.61; H, 6.58; N, 9.14. Found C, 68.55; H, 6.54; N, 9.23. UV-Vis: λ_{max}(Abs) 653 nm, ε 103,000 $M^{-1}cm^{-1}$ (Methanol).

4-((5-(dimethylamino)-1,3,3-trimethyl-3*H*-indol-1-ium-2-yl)methylene)-2-((1-(6-((2,5-dioxopyrrolidin-1-yl)oxy)-6-oxohexyl)-3,3-dimethyl-5-nitroindolin-2-ylidene)methyl)-3-oxocyclobut-1-en-1-olate (4-NHS)

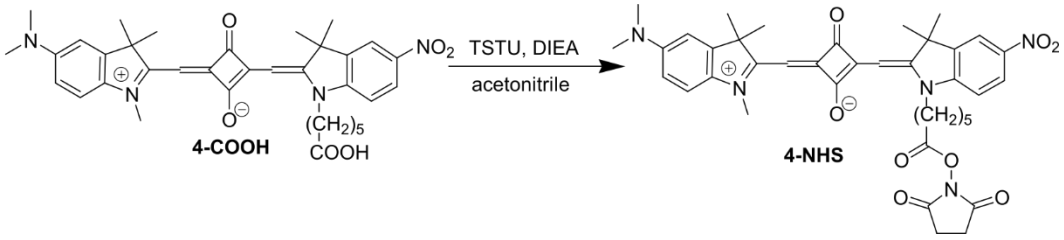

4-COOH (10.5 mg, 17 μmol), *N*,*N*,*N*′,*N*′-tetramethyl-*O*-(*N*-succinimidyl)uronium tetrafluoroborate (TSTU) (9.5 mg, 31 μmol) were dissolved in acetonitrile (1 mL) and dioxane (1.4 mL), and then *N*,*N*-diisopropylethylamine (DIEA) (20 μL, 114 μmol) was added. The solution was stirred at room temperature for 10 min. The solvent was removed under reduced pressure by a rotary evaporator. The residue was purified by a column chromatography (Silica gel 60, 0–3% methanol—chloroform) to give **4-NHS**. Yield: 5.3 mg (44 %). ^{1}H-NMR (200 MHz, DMSO-d_6), δ, ppm: 8.24 (1H, s, arom.), 8.19 (1H, d, 8.0 Hz, arom.), 7.40 (1H, d, 8.8 Hz, arom.), 7.24 (1H, d, 8.1 Hz, arom.), 7.01 (1H, s, arom.), 6.74 (1H, d, 7.8 Hz, arom.), 5.93 (1H, s, CH), 5.72 (1H, s, CH), 3.94 (1H, t, 7.4 Hz, NCH_2), 3.74 (3H, s, NCH_3), 2.98 (6H, s, $N(CH_3)_2$), 2.82 (4H, s, CH_2(succinimide)), 2.69 (2H, t, 7.3 Hz, $C\underline{H}_2COONHS$), 1.76–1.30 (6H, m CH_2), 1.71 (6H, s, $(CH_3)_2$), 1.69 (6H, s, $(CH_3)_2$). ESI MS, m/z calcd. for $[M+H]^+$ $[C_{39}H_{44}N_5O_8]^+$ 710.32, found: 710.48. Anal. calcd. (%) for $C_{39}H_{43}N_5O_8$: C, 65.99; H, 6.11; N, 9.87. Found C, 65.93; H, 6.09; N, 9.89.

2. Squaraine Labeled and Unlabeled DNA Oligonucleotide Sequences and Characterization of Squaraine Labeled DNA Oligonucleotides

Dye-labeled and unlabeled DNA oligonucleotide strands used to form DNA Holliday junctions are listed in **Table S1**.

Table S1. Oligonucleotide sequences used to form Holliday junctions.

Strand	Oligonucleotide Sequence
A	5'-ATA TAA TCG CTC G**T*dye**\C ATA TAA TGA CTG-3'
B	5'-CAG TCA TAA TAT GT GGA ATG TGA GTG-3'
C	5'-CAC TCA CAT TCC AC TCA ACA CCA CAA-3'
D	5'-TTG TGG TGT TGA GC GAG CGA TTA TAT-3'

Mass spectra, provided by Integrated DNA Technologies, Inc. (Coralville, IA), confirm that the squaraines are attached to the oligonucleotides (**Figure S1**).

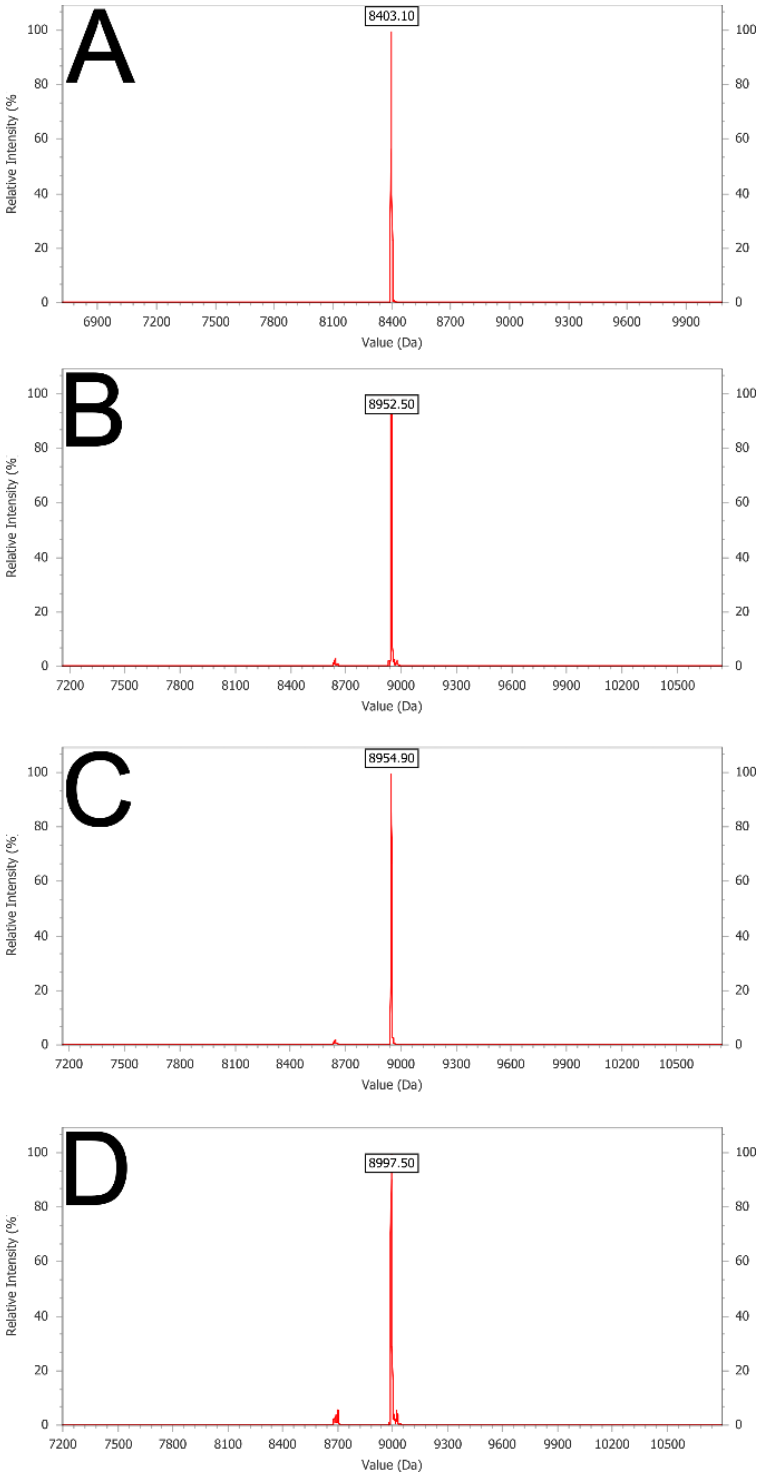

Figure S1. Mass spectra of **1**-**4** (**A**-**D**, respectively) covalently attached to oligonucleotide A (see e.g. **Table S1**). (**A**) The predicted *m*/*z* for A-**1** was 8402.6, the measured *m*/*z* was 8403.1. (**B**) The predicted *m*/*z* for A-**2** was 8952.4, the measured *m*/*z* was 8952.5. (**C**) The predicted *m*/*z* for A-**3** was 8954.4, the measured *m*/*z* was 8954.9. (**D**) The predicted *m*/*z* for A-**4** was 8997.4, the measured *m*/*z* was 8997.5.

3. Representative Visible and Near-Infrared Continuum Probe Spectra

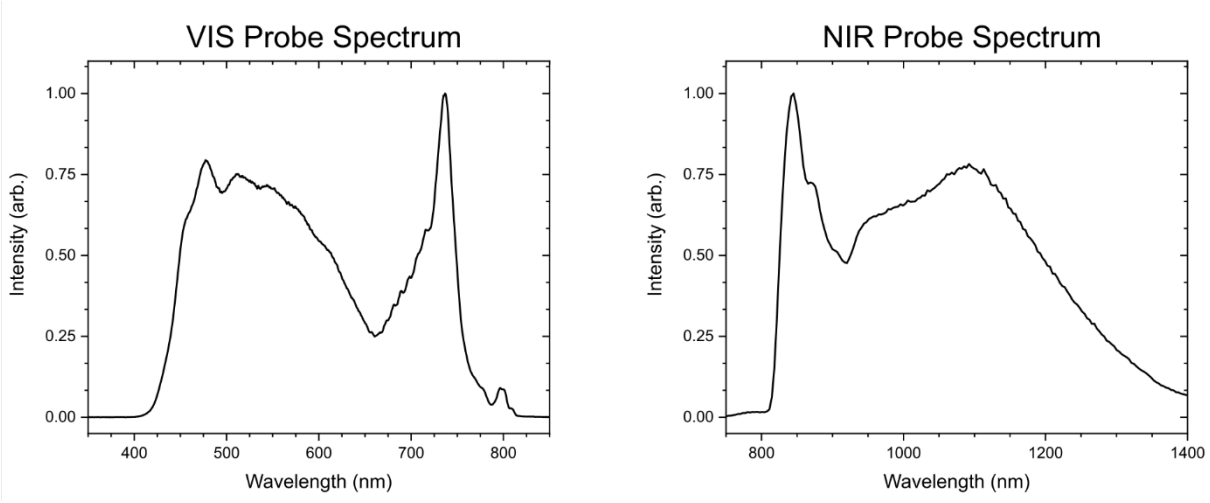

Figure S2. Representative visible and near-infrared continuum probe spectra used in femtosecond visible and near-infrared transient absorption measurements.

4. Suppressing Squaraine Aggregation: Large Average Distance between DNA-Tethered Squaraine Monomer Constructs in Solution

Squaraines have a propensity to aggregate in solution. And so, strategies are needed to suppress aggregation so that the monomer photophysics can be characterized in the absence of squaraine aggregation. We chose to suppress squaraine aggregation by tethering individual squaraine dyes to a DNA Holliday junction (HJ), a large biomolecule that is roughly planar with a length × width of ~10 nm × ~10 nm based on DNA extension. Squaraine aggregation is suppressed by tethering the squaraine to the DNA HJ for the following reasons: (i) the DNA HJ is expected to sterically hinder the aggregation of squaraine dyes, which are much smaller in size (i.e., ~2 nm), and (ii) the DNA HJ will diffuse very slowly, which will act to suppress squaraine aggregation. Additionally, the average distance between dyes, i.e., ~70 (200) nm for the highest (lowest) concentrations used in the measurements of 5 (0.2) μM is much larger than either the size of the dye or the DNA HJ. For these reasons, we expect squaraine aggregation to be suppressed such that the monomer photophysics can be characterized.

5. Tethering the Squaraines to DNA With a Long and Flexible Tether is Not Expected to Alter Their Intrinsic Photophysics

Tethering the squaraines to DNA with a long and flexible tether is not expected to alter their intrinsic photophysics, largely because the dyes are expected to have appreciable conformational freedom. Specifically, **Figure 1B** in the main text displays the structure of the modified thymine base (T*) used to attach the squaraines to DNA. T* is long and, as a result of a large number of single bonds in the structure, is expected to be flexible. In addition to T*, there are five methylene groups bridging the nitrogen atom of the squaraine and the site of attachment to T* (see e.g. **Figure 1A** in the main text). Beginning from the 3' carbon atom of the pentose ring and ending at the nitrogen atom of the squaraine, there are fourteen carbon-carbon single bonds, seven carbon-nitrogen single bonds, and two carbon-carbon double bonds. Assuming the linker takes on a fully trans, anti configuration, that these bond lengths can be approximated as 1.5, 1.4, and 1.3 Å, respectively, and that the bond angles associated with the sp^3 and sp^2 hybridized atoms can be approximated as 109.5 and 120 º, respectively, a value of ~27.8 Å or ~2.8 nm is estimated for the distance from the 3' carbon atom of the pentose ring to the nitrogen atom of the squaraine. This is nearly 50% longer than the squaraine, which is ~2 nm long (see e.g. ref. 2) in its trans, anti conformation (see e.g. ref. 3). Thus, the length of the linker is larger than that of the squaraine. Due to the length and flexibility of the linker, we expect the squaraine to have appreciable conformational freedom. That is, the squaraine can sample a range of: (i) orientations, i.e., rotational motion about bonds within the squaraine is not severely inhibited, and (ii) solvent environments, including the aqueous buffer and/or DNA environment. As such, we expect the intrinsic photophysics of the squaraines are not modified by their attachment to DNA.

6. Experimental Extinction Spectra of DNA-Tethered Squaraine Monomer Solutions

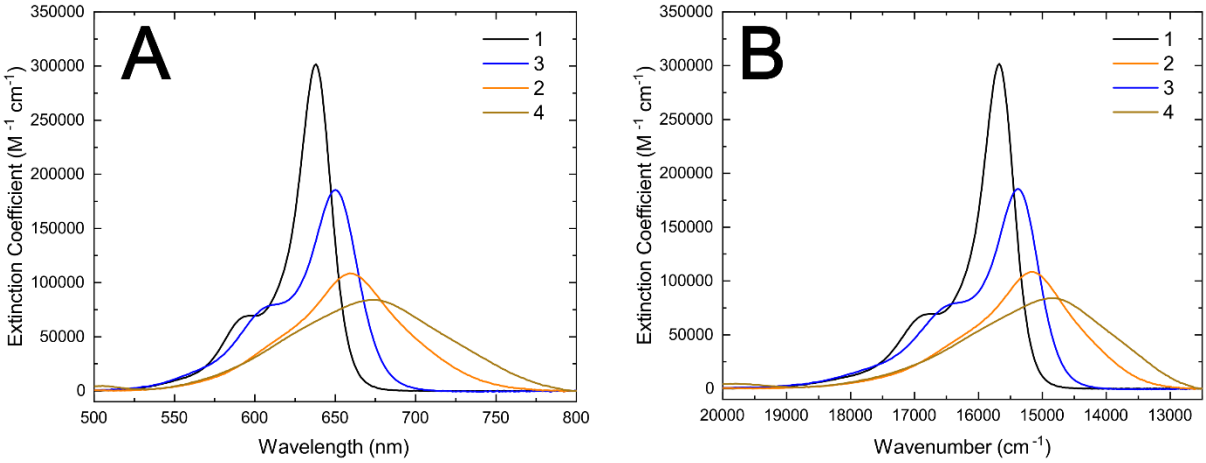

Figure S3. Extinction spectra of DNA-tethered squaraines **1**-**4** in aqueous buffer solution plotted in units of (**A**) wavelength and (**B**) wavenumber (cm^{-1}). The transition dipole moment μ is determined by integrating under the curve of the plots in (**B**). Despite the decrease in the peak extinction coefficients of **2** and **3**, a large transition dipole moment is maintained via the broadening of their extinction spectra. The transition dipole moments of **1**-**4** are quantified in **Table 2** in the main text.

7. Fluorescence Quantum Yield Measurements of DNA-Tethered Squaraine Monomer Solutions

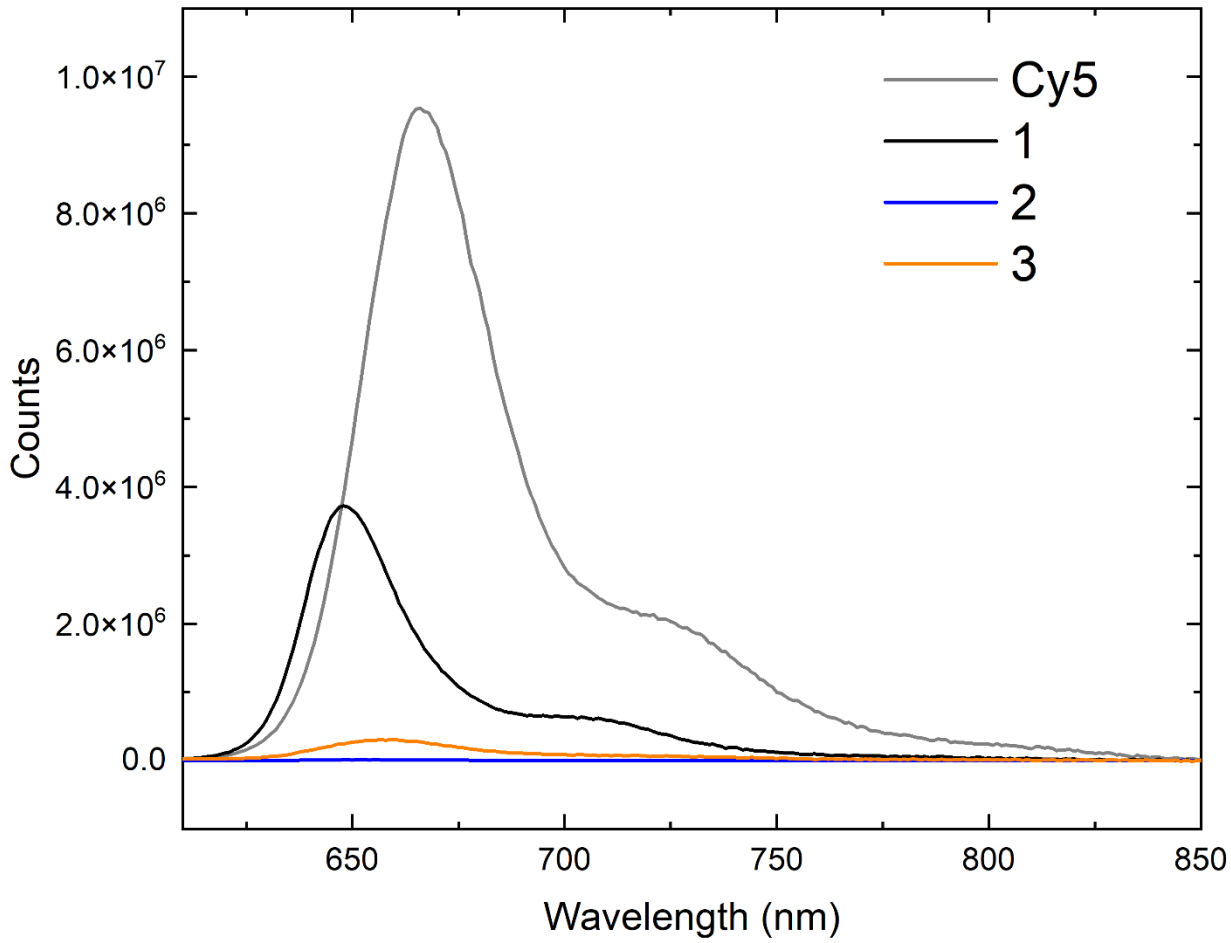

Figure S4. Steady-state fluorescence emission spectrum of the DNA-duplex tethered cyanine dye Cy5 (Φ_F = 0.29, see e.g. [S4]), which was used as the relative fluorescence quantum yield (FQY) standard, overlaid with the corresponding steady-state fluorescence emission spectra of DNA Holliday junction-tethered **1**-**3** used to determine their FQY. The latter were dissolved in an aqueous buffer including 1× TBE 15 mM $MgCl_2$. See the main text for additional details on how the FQY was calculated.

8. Analysis of TCSPC Decay Kinetics of DNA-Tethered Squaraine Monomer Solutions

The fluorescence decay of **1** was fit with a single exponential decay term, as the data appeared to decay monotonically upon initial inspection. A single exponential term provided an adequate fit for **1**, as evidenced by good agreement with the data and minimal structure in the residual (**Figure S5**). Furthermore, a single exponential fit is physically reasonable, as steady-state fluorescence measurements had previously indicated that solutions of **1** were homogeneous.

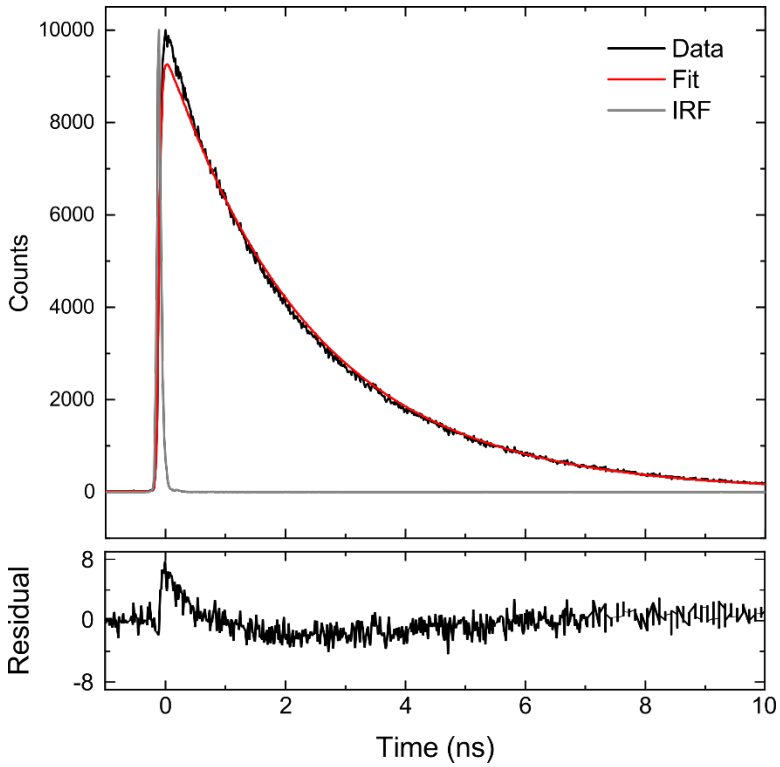

Figure S5. The data, shown in black, and fits, shown in red, resulting from a single exponential fit of the TCSPC decays of **1.** The instrument response function is shown in gray. The bottom plot shows the residuals from the fit. The detection wavelength was 700 nm.

Upon initial inspection, the fluorescence decays of **2** and **3** each indicate an initial, rapid decay followed by a much slower decay to baseline (**Figure S6**). The observation of multiple decay components is especially clear in **3**, where the decay trace resembles the IRF until ~100 ps before slowly decaying to baseline. These observations indicated that a single exponential term would be insufficient to adequately describe the data, so the fluorescence decays of **2** and **3** were fit with two exponential terms. The bi-exponential analysis described the data well, as evidenced by the good agreement and minimal structure in the residuals. The derived amplitudes and time constants are shown in **Table 4** in the main text.

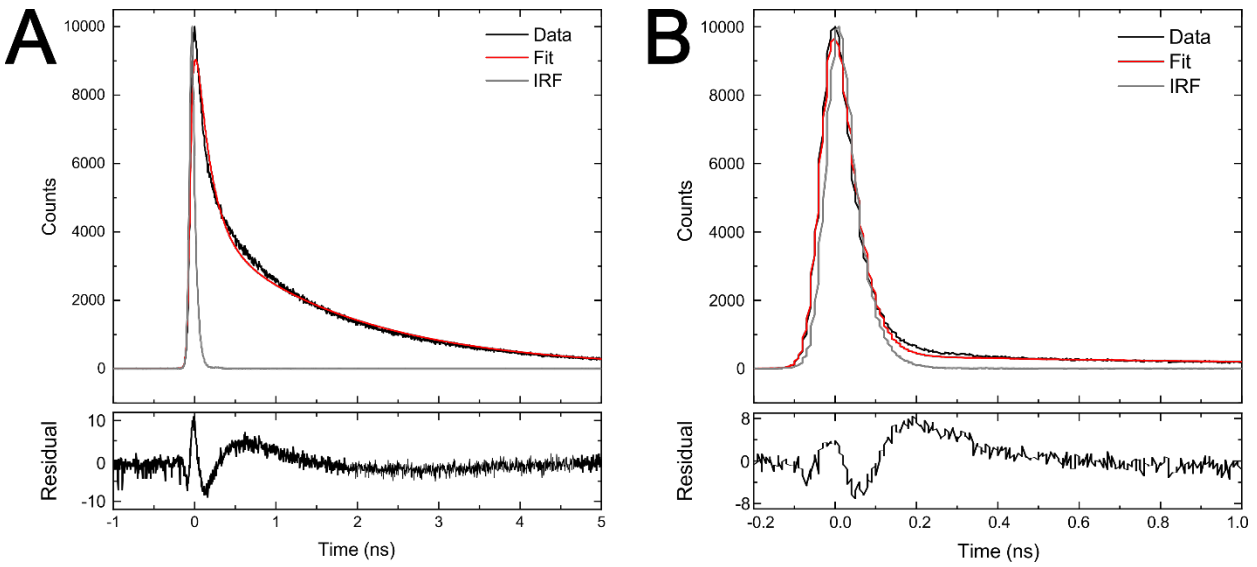

Figure S6. The data, shown in black, and fits shown in red resulting from a bi-exponential fit of the TCSPC decays of (A) **2** and (B) **3**. The instrument response function is shown in gray. The bottom plot shows the residuals from the fit. The detection wavelength for both measurements was 700 nm.

Steady-state fluorescence measurements had previously indicated that solutions of **2** and **3** were heterogeneous. Therefore, the additional component in the TCSPC decay kinetics in solutions of **2** and **3** is attributed to a small subpopulation of long-lived dyes in solutions of **2** and **3**.

9. Mathematical and Physical Justification of Number of Components for Fitting Femtosecond Visible Transient Absorption of DNA-Tethered Squaraine Monomer Solutions

When performing the global target analysis (GTA) of the transient absorption (TA) of solutions of **1**-**3**, the results of the TCSPC analysis (**Section S8**) informed the choice of the number of kinetic components for the initial GTA of each solution. In the TCSPC analysis, solutions of **1** were well described by a single exponential, so a one-component GTA was used for the TA of solutions of **1**. Excellent agreement between the data and fit, evidenced by minimal structure in the residuals, indicate that solutions of **1** are well described by a single component GTA (**Figure S7**). The lifetime of 2.4 ns derived by the single component GTA also agrees with the value measured by TCSPC.

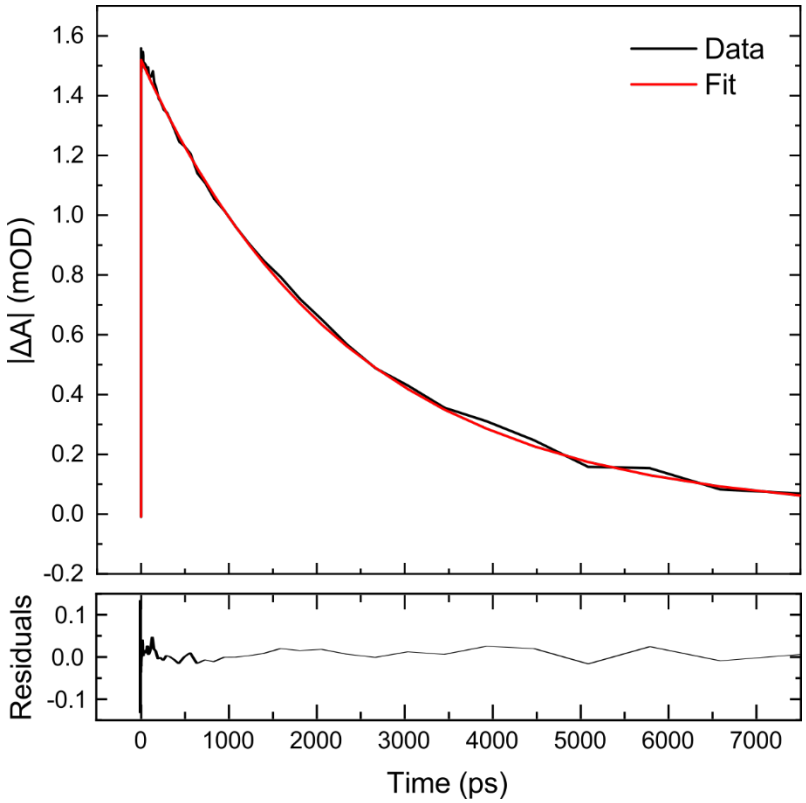

Figure S7. The kinetic trace of the ground state bleach (600 nm) of solutions of **1** excited at 640 nm, analyzed with a one-component GTA. Data is plotted in black and the fit is plotted in red. The fit residuals are shown below the plot.

For the TCSPC of **2**, the solutions were excited at 660 nm, which excites the non-protonated form of **2** along with a small subpopulation of long-lied dyes. Analysis of the TCSPC returned an IRF-limited time constant assigned to the non-protonated form of **2** and a second time constant assigned

to a small subpopulation of long-lived dyes. For the TA of solutions of **2** excited at 700 nm, only the non-protonated population of **2** is excited, therefore a GTA was initially performed using a single component. A kinetics trace at 640 nm and the single component fit are overlaid in the left panel of **Figure S8**. As evidenced by poor agreement between data and fit at early times, a single component was insufficient to describe the dynamics of **2**. Accordingly, the analysis was repeated with the addition of a second component, which significantly improved the fit. Therefore, two time constants were necessary to describe the dynamics of the non-protonated form of **2**. Physical assignments of the two time constants can be found in the main text.

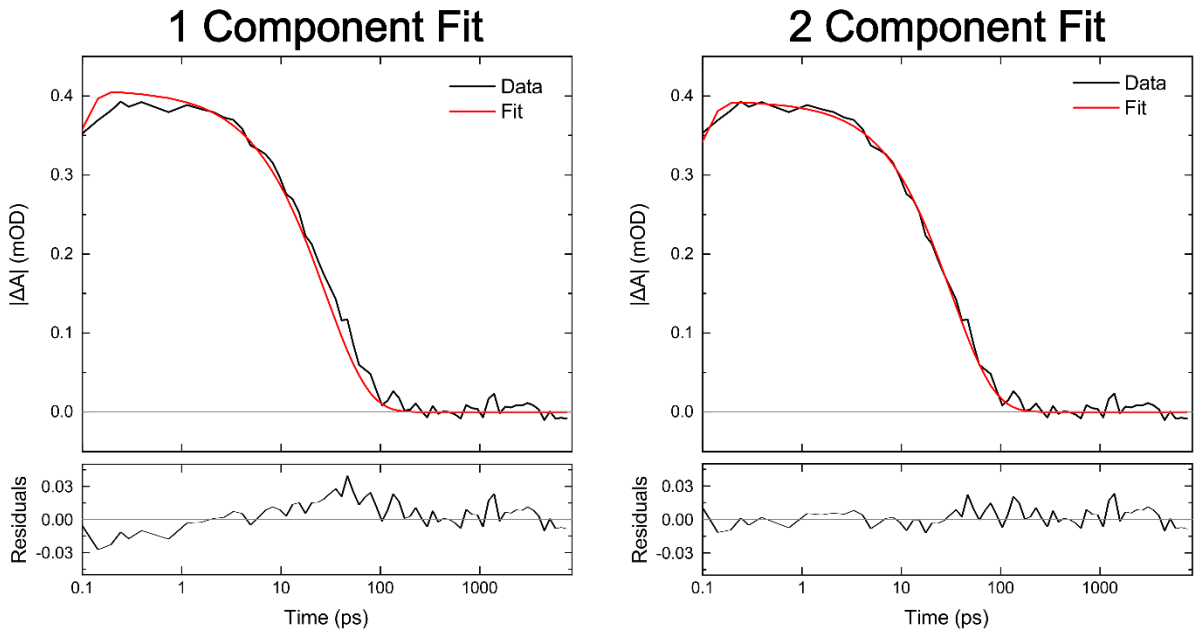

Figure S8. The kinetics traces of the ground state bleach (640 nm) of solutions of **2** excited at 700 nm, analyzed with one- and two-component GTA (left and right, respectively). Data are plotted in black and fits are plotted in red. The fit residuals are shown below each plot. A logarithmic scale is used for the time axis to better visualize the early-time kinetics.

Guided by the GTA of solutions of **2** pumped at 700 nm, two components were initially used for the analysis of solutions of **2** pumped at 650 nm. While the two-component GTA returned two short time constants that described the early-time behavior well, it did not accurately capture the long-time dynamics of solutions of **2** (**Figure S9**). A third component, decaying in parallel and fixed to the long-lived time constant derived by TCSPC analysis, was incorporated into the GTA and led to excellent agreement between the data and fit, as can be seen in the right panel of **Figure S9**.

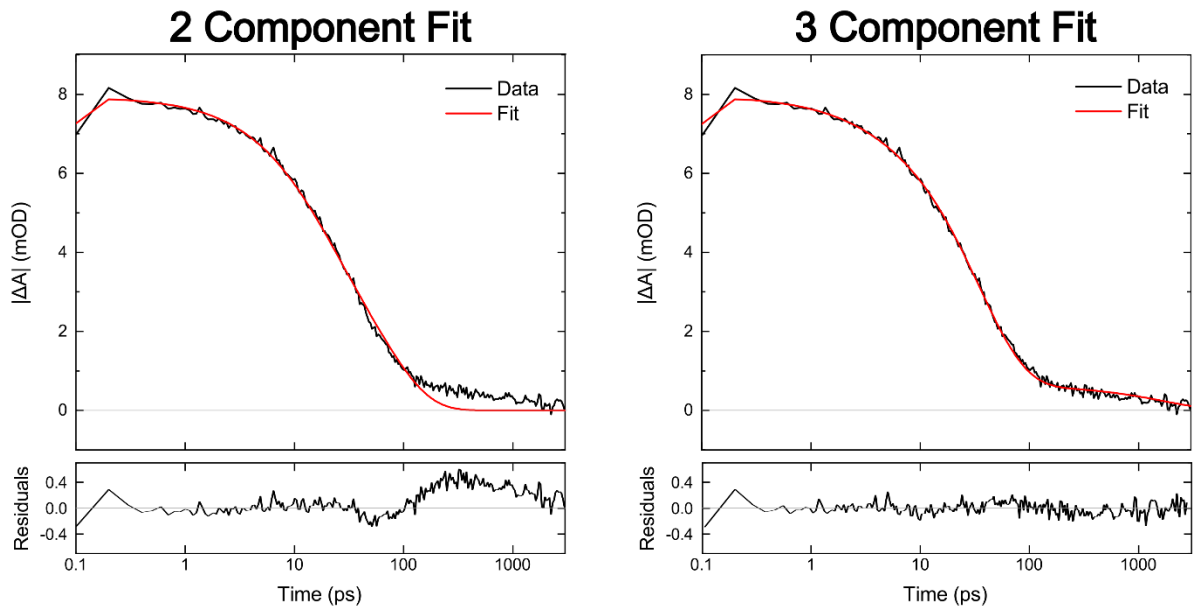

Figure S9. The kinetics traces of the ground state bleach (640 nm) of solutions of **2** excited at 650 nm, analyzed with two- and three-component GTA (left and right, respectively). Data are plotted in black and fits are plotted in red. The fit residuals are shown below each plot. A logarithmic scale is used for the time axis to better visualize the early-time kinetics.

The physical assignment of the three time constants returned by GTA of the TA of solutions of **2** excited at 650 nm is aided by examining the species associated difference spectra (SADS), which are plotted in **Figure S10**. In the figure, SADS-1 and SADS-2 resemble the two SADS from solutions of **2** pumped at 700 nm (**Figure 10**) and the calculated lifetimes are comparable. Therefore, the first two SADS are assigned to the excited-state dynamics of the non-protonated form of **2**. SADS-3 has distinct excited-state absorption (ESA) bands at ~480 and 540 nm, a ground state bleach (GSB) band at ~620 nm, and stimulated emission (SE) bands at ~700 nm (**Figure S10**, right panel), which resembles the TA spectrum of **1**. Additionally, the GSB of SADS-3 is blue-shifted from that of SADS-1 and SADS-2, reminiscent of the blue-shift of the absorption of the protonated form of **2** relative to that of the non-protonated form of **2** (**Figure 4**). Because of these spectral features, and the long time constant associated with the SADS, SADS-3 is assigned to a subpopulation of long-lived dyes, resembling the protonated form of **2**. Additionally, the small amplitude of SADS-3, indicates that the subpopulation is a minor subpopulation in the solution, despite absorbing strongly at the excitation wavelength of 650 nm.

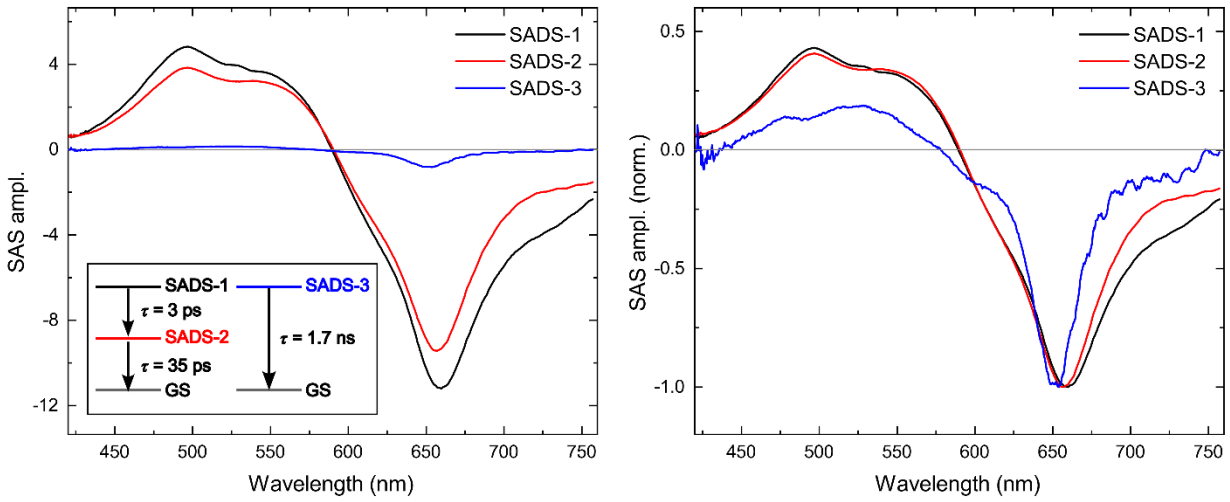

Figure S10. The species associated difference spectra (SADS) of solutions of **2** excited at 650 nm, analyzed with a three-component GTA. The SADS are plotted on the left to facilitate comparison of SADS amplitudes, and normalized SADS are plotted on the right to facilitate comparison between spectral features of the SADS. The inset displays the kinetic scheme and time constants associated with each transition.

GTA of solutions of **3** was guided by the TCSPC analysis, which derived an IRF-limited time constant assigned to the excited state dynamics of **3** and a longer time constant assigned to a small, long-lived subpopulation. As such, a two-component GTA was attempted on the TA of solutions of **3** using TCSPC-derived time constants as an initial guess. The GTA produced a fit that did not describe the early-time decay well, as evidenced by poor agreement between data and fit between 0.1 and 10 ps (**Figure S11**). A third component was added to the fit, which improved the agreement between data and fit at early times. Physical assignment of the two short time constants associated with SADS-1 and SADS-2 can be found in the main text. As with solutions of **2**, SADS-3 resembles the TA spectrum of **1** and has a long lifetime, thus it is assigned to a small subpopulation of a long-lived dyes (**Figure S12**).

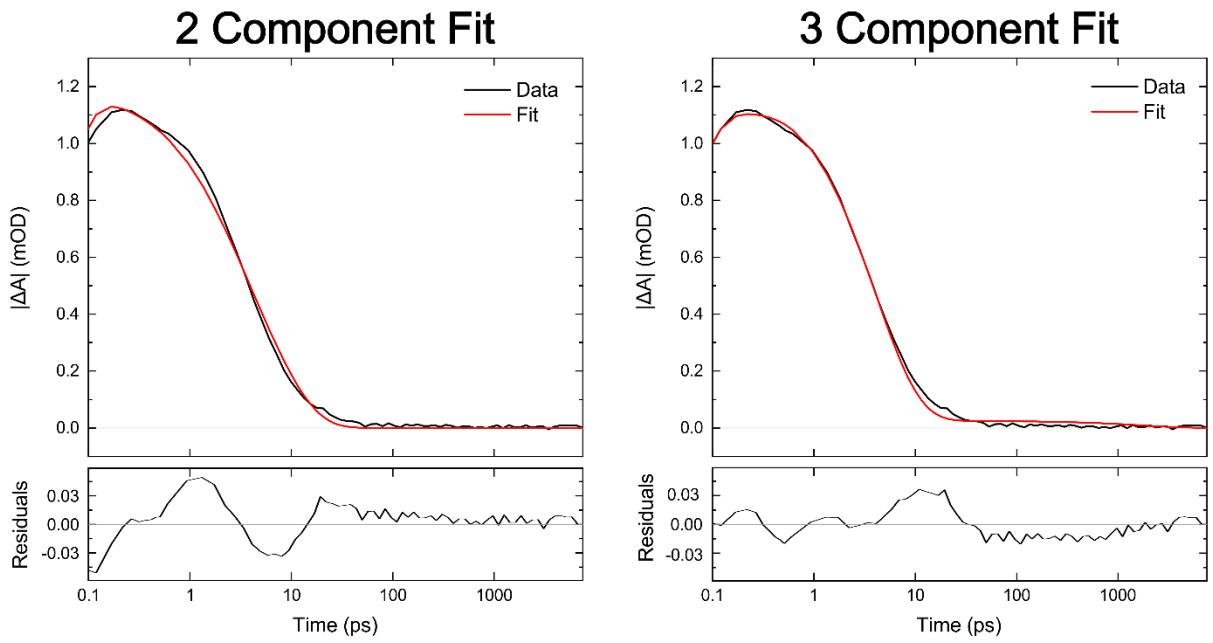

Figure S11. The kinetics traces of the ground state bleach (610 nm) of solutions of **3** excited at 650 nm, analyzed with two- and three-component GTA (left and right, respectively). Data are plotted in black and fits are plotted in red. The fit residuals are shown below each plot. A logarithmic scale is used for the time axis to better visualize the early-time kinetics.

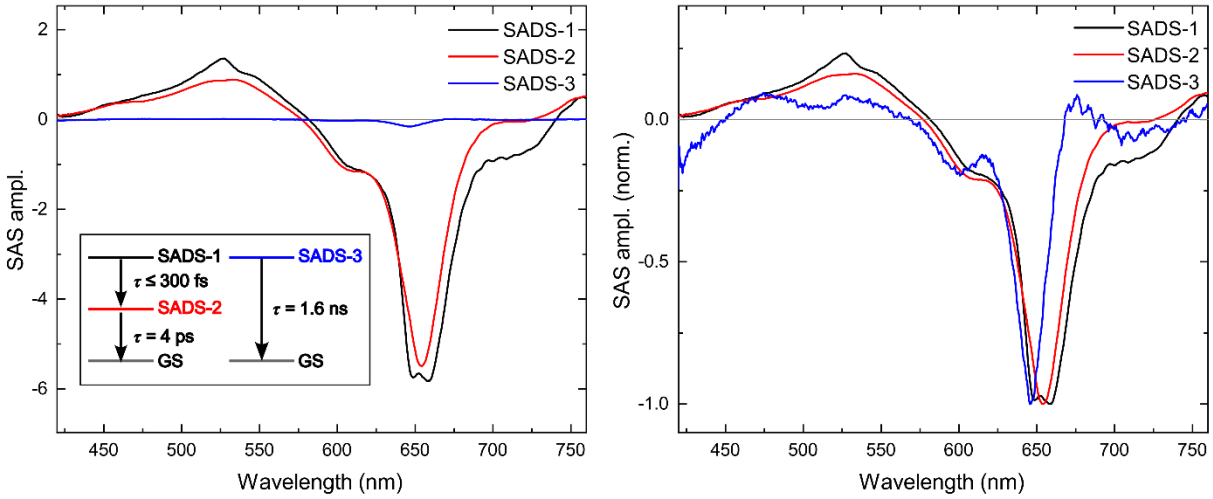

Figure S12. The species associated difference spectra (SADS) of solutions of **3** excited at 650 nm, analyzed with a three-component GTA. The SADS are plotted on the left to facilitate comparison of SADS amplitudes, and normalized SADS are plotted on the right to facilitate comparison between spectral features of the SADS. The inset displays the kinetic scheme and time constants associated with each transition.

10. Supporting References

1. Gottlieb, H. E., Kotlyar, V. & Nudelman, A. NMR Chemical Shifts of Common Laboratory Solvents as Trace Impurities. *J. Org. Chem.* **62**, 7512–7515 (1997).
2. Lynch, D. E., Kirkham, A. N., Chowdhury, M. Z. H., Wane, E. S. & Heptinstall, J. Water soluble squaraine dyes for use as colorimetric stains in gel electrophoresis. *Dyes Pigments* **94**, 393–402 (2012).
3. Barcenas, G. *et al.* First-principles studies of substituent effects on squaraine dyes. *RSC Adv.* **11**, 19029–19040 (2021).
4. Huff, J. S. *et al.* DNA-Templated Aggregates of Strongly Coupled Cyanine Dyes: Nonradiative Decay Governs Exciton Lifetimes. *J. Phys. Chem. Lett.* **10**, 2386–2392 (2019).